

Cumulant expansion for phonon contributions to the electron spectral function

S. M. Story,¹ J. J. Kas,¹ F. D. Vila,¹ M. J. Verstraete,² and J. J. Rehr¹

¹*Department of Physics, University of Washington Seattle, WA 98195*

²*Institut de Physique, Université de Liège B-4000 Sart Tilman, Belgium*

(Dated: July 25, 2014)

We describe an approach for calculations of phonon contributions to the electron spectral function, including both quasiparticle properties and satellites. The method is based on a cumulant expansion for the retarded one-electron Green's function and a many-pole model for the electron self-energy. The electron-phonon couplings are calculated from the Eliashberg functions, and the phonon density of states is obtained from a Lanczos representation of the phonon Green's function. Our calculations incorporate *ab initio* dynamical matrices and electron-phonon couplings from the density functional theory code ABINIT. Illustrative results are presented for several elemental metals and for Einstein and Debye models with a range of coupling constants. These are compared with experiment and other theoretical models. Estimates of corrections to Migdal's theorem are obtained by comparing with leading order contributions to the self-energy, and are found to be significant only for large electron-phonon couplings at low temperatures.

I. INTRODUCTION

To first approximation, electronic and vibrational properties can be treated separately in condensed matter due to the large mass ratio between electrons and ions, e.g., within the Born-Oppenheimer approximation. However, corrections to this approximation, which depend on the strength of the electron-phonon interaction, are of considerable importance both theoretically and experimentally. Here we investigate the effects of electron-phonon interactions on the quasiparticle properties of electrons. Due to such interactions, the electron energy levels ε_k are not sharply defined, but have finite lifetimes characterized by the electron self-energy Σ , which lead to broadening of the associated spectral function. Such effects are visible experimentally, e.g., in high resolution ARPES spectra at low temperatures.¹

In general, the electron spectral function is dominated by a sharp quasiparticle peak, but it can also exhibit satellites due to phonon excitations. According to Migdal's theorem,² only the leading order electron-phonon interaction contributions to the self-energy are important, due to the large mass ratio between electrons and nuclei. In that case, the electron self-energy can be approximated by the simplest diagram, and vertex corrections can be neglected. This approximation has been investigated in detail³⁻⁷ and extended to finite temperature, e.g., by Allen.⁸ The Migdal approximation is analogous to the *GW* approximation of Hedin⁹ for electrons coupled to plasmons where G is the electron Green's function and W the screened Coulomb interaction. Since a similar formalism applies to phonons, electron-hole pairs and other neutral bosonic excitations, we will refer to this leading order diagram as the *GW* approximation. The *GW* theory leads to spectral functions with a quasiparticle peak and two satellite features originating from single-boson excitations, one on each side of the main quasiparticle peak.

In contrast to the *GW* approximation, however, systems of electrons coupled to neutral bosonic excitations

generally exhibit multiple satellites, as observed in photoemission experiments.^{10,11} Moreover, the *GW* approximation is known to be unsatisfactory for describing satellite structures, as the satellite peaks typically appear at the wrong energies and with the wrong intensities compared to experiment. Thus, it is of interest to investigate possible corrections to Migdal's theorem, i.e., the effects of higher order terms in an expansion in powers of the electron-phonon coupling.¹² One approach to this end is to investigate contributions to the self-energy from the vertex function Γ , as in the formal identity $\Sigma = iGWT$. However, direct calculations of Γ have been formidably challenging, and there has been little progress along these lines. An attractive alternative that overcomes some of the shortcomings of *GW* is provided by the cumulant expansion,¹²⁻¹⁴ which is an exponential representation of the electron Green's function in the time domain. The cumulant expansion is exact for the case of a deep core-level coupled to bosons, and generalizations have been developed for valence electrons coupled to plasmons.^{15,16} The approach has been applied with considerable success in many cases, ranging from multiple plasmon satellites in photoemission¹⁷ to dynamical mean field theory.¹⁸ Nevertheless, the conventional approach based on the time-ordered Green's function is only strictly applicable for the hole- or particle-branch of the spectral function depending on whether the state is above or below the Fermi level. This limitation is particularly problematic in systems with particle-hole symmetry, such as electrons coupled to phonons. To overcome this difficulty, we utilize here the recently developed retarded cumulant (RC) approach, which is based on a particle/hole cumulant and a *retarded* Green's function formalism.¹⁴ A further goal of the present work is to develop a practical approach for calculations of phonon contributions to properties of condensed matter.

The remainder of this paper is organized as follows. In Sec. II, we describe the retarded cumulant expansion method and many-pole model self-energy used to calculate phonon contributions to the electron spectral func-

tion. Sec. III gives details on how this method is implemented computationally with our workflow tool AI2PS. Finally, our results are presented in Sec. IV, and Sec. V contains a summary and conclusions.

II. THEORY AND METHODOLOGY

In this section, we briefly summarize the GW and RC approximations for calculations of the electron spectral function in systems linearly coupled to phonons. As usual, the Hamiltonian for the electron-phonon system is represented as

$$H = \sum_k \varepsilon_k^0 c_k^\dagger c_k + \sum_q \omega_q a_q^\dagger a_q + \sum_{kk'q} V_{kk'}^q (a_q + a_q^\dagger) c_k^\dagger c_{k'}, \quad (1)$$

where k denotes the electron levels and q the phonon modes with bare energies ε_k^0 and ω_q respectively, $V_{kk'}^q$ are the electron-phonon matrix elements, and c_k (c_k^\dagger) and a_q (a_q^\dagger) are the electron and phonon destruction (creation) operators. In this paper, we use atomic units $e = \hbar = m = 1$ and $k_B = 0.086173$ meV/K. At low temperatures, the electrons are nearly degenerate with Fermi energy ε_F and $\omega_q \ll \varepsilon_F \ll \omega_p$, where ω_p is the dominant plasmon excitation energy, which is typically several eV. Thus, for our purposes here, the density of electron states near ε_F replaced by a constant, which we assume is non-vanishing. The generalization to insulators or molecular systems with discrete spectra near ε_F is straightforward, but will not be treated here.

A. GW spectral function

Schematically, the GW approximation for the self-energy is given by $\Sigma = iGW$, where G is the one-electron Green's function and W is an approximation for the screened Coulomb interaction. Within GW, the usual strategy is to calculate the spectral function $A_k(\omega)$ from the imaginary part of the one-electron Green's function in frequency space,³

$$\begin{aligned} G_k(\omega) &= \frac{1}{\omega - \varepsilon_k^0 - \Sigma_k(\omega)} \\ A_k(\omega) &= \frac{1}{\pi} |\text{Im } G_k(\omega)| \\ &= \frac{1}{\pi} \frac{|\text{Im } \Sigma_k(\omega)|}{|\omega - \varepsilon_k^0 - \text{Re } \Sigma_k(\omega)|^2 + |\text{Im } \Sigma_k(\omega)|^2}. \end{aligned} \quad (2)$$

The spectral function is comprised of two main features—a dominant quasiparticle peak at $\omega = \varepsilon_k = \varepsilon_k^0 + \Sigma_k$ with width $\text{Im } \Sigma_k$ and phonon satellites at $\omega = \varepsilon_F \pm \omega_q$, consistent with Ref. 3. Other physical properties such as the quasiparticle lifetime and energy levels can be obtained from the properties of $A_k(\omega)$ and $\Sigma_k(\omega)$.

B. RC spectral function

As noted in the introduction, the conventional time-ordered cumulant expansion must be generalized to treat cases with particle-hole symmetry, such as phonon excitations in metals.¹² Our treatment is based on the RC formalism which is discussed in detail by Kas et al.¹⁴ For a degenerate Fermi system in the absence of plasmons, the RC representation of the retarded one-particle Green's function is

$$\begin{aligned} G_k^R(t) &= G_k^{0,R}(t) e^{C_k^R(t)} \\ G_k^{0,R}(t) &= -i e^{-i\varepsilon_k^0 t} \theta(t), \end{aligned} \quad (3)$$

where $C_k^R(t)$ is the cumulant as described below. Formally, the spectral function is obtained from a Fourier transform

$$A_k(\omega) = \text{Im} \int_{-\infty}^{\infty} \frac{dt}{2\pi} i e^{i\omega t} G_k^R(t). \quad (4)$$

The retarded particle/hole cumulant $C_k^R(t)$ is then approximated by the second order (in electron-phonon coupling) cumulant diagram¹⁴

$$\begin{aligned} C_k^R(t) &\approx C_{2,k}^R(t) \\ &= i e^{i\varepsilon_k^0 t} \int_{-\infty}^{\infty} \frac{d\omega}{2\pi} e^{-i\omega t} \left[G_k^{0,R}(\omega) \right]^2 \Sigma_k^R(\omega). \end{aligned} \quad (5)$$

This diagram is conveniently evaluated in frequency space¹⁴ and can be expressed in terms of the imaginary part of the $G^0 W^0$ boson excitation spectrum $\beta_k(\omega)$ as

$$C_k^R(t) = \int_{-\infty}^{\infty} d\omega \beta_k(\omega) \frac{e^{i\omega t} - i\omega t - 1}{\omega^2}, \quad (6)$$

where $\beta_k(\omega)$ is obtained from the GW self-energy

$$\beta_k(\omega) = \frac{1}{\pi} |\text{Im } \Sigma_k(\omega + \varepsilon_k^0)|. \quad (7)$$

Consequently the ingredients in the RC are similar to those in GW and hence the RC is no more difficult to calculate than the GW approximation. In contrast to the conventional time-ordered cumulant expansion, which only contains frequencies within the particle- or hole branches, the retarded cumulant in Eq. (6) contains *all* frequencies, and explicitly builds in the particle-hole symmetry desired for phonons. Also, due to the behavior of the essentially dispersionless self-energy $\Sigma_k(\omega)$, (Fig. 1), multiple phonon satellites may exist with the cumulant expansion, as peaks at integral multiples of ω_E on both sides of the Fermi energy ε_F . This is in contrast to the case with plasmons, where the satellites appear at multiples of ω_p from the quasiparticle peak at ε_k .

C. Many-pole GW self-energy

The dominant ingredient in the RC is the $G^0 W^0$ boson excitation spectrum $\beta_k(\omega)$, which is general for any given

self-energy, but we will focus on a self-energy model appropriate for phonons. Here we have adapted the finite-temperature Einstein model for phonons,^{8,19,20} where the self-energy is represented as a sum over Einstein modes. For a single mode with Einstein frequency ω' , the GW self-energy at finite temperature T (with unit coupling) is given by^{8,20}

$$\Sigma^E(\omega, \omega', T) = -i\pi \left[n(\omega') + \frac{1}{2} \right] + \frac{1}{2}\Psi \left(\frac{1}{2} + i\frac{\omega' - \omega}{2\pi T} \right) - \frac{1}{2}\Psi \left(\frac{1}{2} - i\frac{\omega' + \omega}{2\pi T} \right), \quad (8)$$

where $n(\omega)$ is the Bose-Einstein distribution and $\Psi(z)$ is the digamma function. The electron-phonon coupling constants in the model are represented in terms of the Eliashberg function $\alpha^2 F_k(\omega)$. The self-energy to be used for $\beta_k(\omega)$ in Eq. (7) is then^{8,19}

$$\Sigma_k(\omega, T) = \int d\omega' 2\Sigma^E(\omega, \omega', T) \alpha^2 F_k(\omega'). \quad (9)$$

We emphasize that the form of the self-energy in Eq. (9) is strictly appropriate only for cases where the band width of electron states near the Fermi energy is large compared to characteristic phonon energies ω , and will not work for sharp band features. This is the case for valence states in metals and in many semi-metals, semi-conductors, and insulators, but becomes questionable in the case of small molecules and core level states. Thus in the present work, we focus only on a selection of metallic systems with a range of electron-phonon couplings. As an example, Fig. 1 shows the real and imaginary parts of the self-energy calculated using Eq. (9) from coupling to a single Einstein mode, i.e., an Einstein model for the phonon spectrum in Cu.

Moreover, for computational simplicity, it is convenient to use a many-pole model for the self-energy,³ analogous to the plasmon-pole model of Hedin and Lundqvist.^{22–25} The integration over the phonon frequencies ω' in Eq. (9) can be replaced by a discrete sum over a sufficiently large number of poles without significant loss of accuracy. For the electron-phonon couplings $\alpha^2 F_k(\omega)$, we employ a pole model similar to that used for the dielectric function in Ref. 25. Generally, $\alpha^2 F_k(\omega)$ depends on both k and k' through the electron-phonon matrix elements $g_{kk'}^q$.^{26–29} However, since the phonon spectra involve energies very close to ε_F , it is sufficient for our purposes here to use the Eliashberg function averaged over the Fermi surface

$$\alpha^2 F(\omega) = \frac{1}{2\pi N(\varepsilon_F)} \sum_q \sum_{k, k' \approx \varepsilon_F} |g_{kk'}^q|^2 \delta(\omega - \omega_q) \quad (10)$$

$$g_{kk'}^q = \sum_{\sigma\sigma'} \langle \psi_{\sigma', k'} | \delta V_{kk'}^q | \psi_{\sigma, k} \rangle,$$

where $k = k' + q \approx \varepsilon_F$, $N(\varepsilon_F)$ is the bare density of states at the Fermi level, and σ denotes spin states. Typically, the $\alpha^2 F(\omega)$ spectrum is rather similar to the total phonon

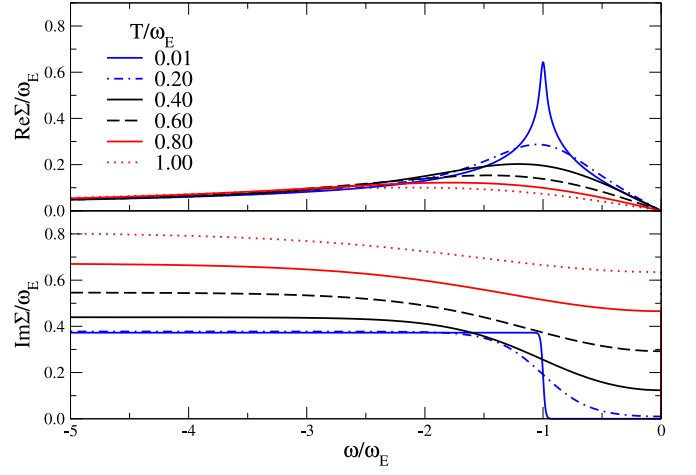


FIG. 1: (color online) Real (top) and imaginary (bottom) parts of the self-energy $\Sigma_k(\omega)$ in Eq. (9) using the Einstein model for Cu, where $\omega_E = 21.6$ meV = 251 K (see text). Positive ω is not shown, as $\text{Re } \Sigma$ and $\text{Im } \Sigma$ and can be obtained from the parity of $\Sigma_k(\omega)$ versus ω .

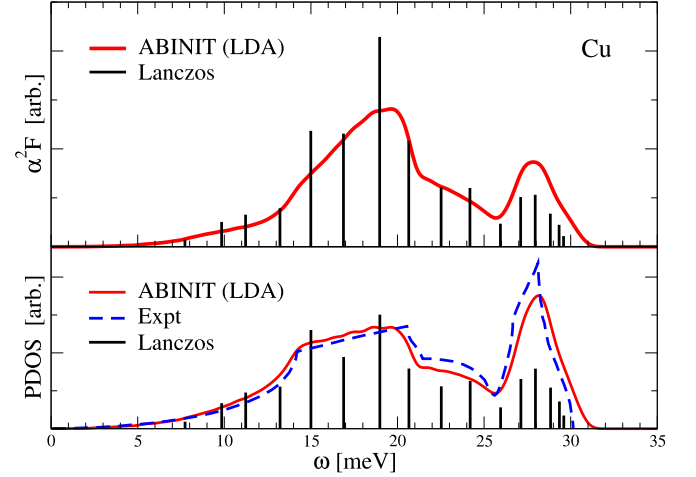


FIG. 2: (color online) Eliashberg function (top) $\alpha^2 F(\omega)$ and total density of modes (bottom) for Cu at the Fermi level $k = k_F$ obtained from ABINIT with our many-pole approximations α_i^2, F_i calculated by the Lanczos inversion tools in FEFF9 (see text). Experimental PDOS taken from Ref. 21. Calculated frequencies have been scaled to match the peak frequency with experiment.

density of states (PDOS) $F(\omega)$ in the system (see Fig. 2), for which an efficient many-pole Lanczos representation has been developed,³⁰

$$F^{\text{MP}}(\omega) = \sum_i F_i \delta(\omega - \omega_i). \quad (11)$$

Thus, a many-pole representation of $\alpha^2 F^{\text{MP}}$ can be constructed similarly,

$$\alpha^2 F^{\text{MP}}(\omega) = \sum_i \alpha_i^2 F_i \delta(\omega - \omega_i). \quad (12)$$

Here the amplitudes

$$\alpha_i^2 = \alpha^2 F(\omega_i) / F(\omega_i) \quad (13)$$

represent the discretized electron-phonon couplings. A 16-pole representation of the copper Eliashberg function is shown in Fig. 2. Finally, an effective or mean electron-phonon coupling constant λ can be defined, which is related to the first inverse frequency moment of the Eliashberg function³¹

$$\lambda = 2 \int_0^\infty \frac{d\omega}{\omega} \alpha^2 F(\omega) \approx 2 \sum_i \frac{\alpha_i^2 F_i}{\omega_i}. \quad (14)$$

This quantity provides a dimensionless characterization of the strength of electron-phonon coupling in a given material.

III. IMPLEMENTATION

The calculations of phonon properties presented here were carried out using AI2PS (*ab initio* DFT to Phonon Spectra),³² a workflow tool we have developed that links density functional theory electronic structure codes, ABINIT in this case,^{33,34} to the vibrational properties module of real-space Green's function code FEFF9.³⁵ AI2PS can be used to calculate phonon properties such as Debye-Waller factors in x-ray spectra. The modular interface automatically coordinates the desired workflow. Briefly, for our purposes here, AI2PS uses ABINIT to generate a set of real-space symmetry-inequivalent blocks of the lattice dynamical matrix (DM), which are used to calculate the many-pole PDOS $F^{\text{MP}}(\omega)$.³⁰ The code ABINIT also yields both $F(\omega)$ and $\alpha^2 F(\omega)$, which are used to calculate the couplings $\alpha^2(\omega)$ using Eq. (13). Since Eq. (9) is restricted to energies near the Fermi level, this presently excludes any k -dependent features in the spectral functions presented in the current study. The ABINIT calculations used Troullier-Martins/Fritz Haber Institut LDA pseudopotentials, and an energy cutoff of 50 Hartrees; for convergence of $\alpha^2 F(\omega)$, a $32 \times 32 \times 32$ Monkhorst-Pack k -point grid was found to be necessary. For the metallic systems discussed here, the occupation numbers were smeared with the Methfessel and Paxton scheme³⁶ with a broadening parameter of 0.025. Run-times were dominated by the ABINIT portion of the workflow. Using 160 AMD Opteron 6128 (800 MHz) cores spread across ten nodes, the runtime for one set of parameters is split roughly 99% (~ 200 minutes) ABINIT for the coupling constants and 1% (~ 2 minutes) FEFF9 for the vibrational properties. Calculations of the spectral function $A_k(\omega)$ were parameterized by the quasiparticle energy $\varepsilon_k = \varepsilon_k^0 + \text{Re}\Sigma_k(\varepsilon_k^0)$ instead of ε_k^0 (see Eq. (3) and (7)). This further simplified the calculation by removing self-energy shifts.

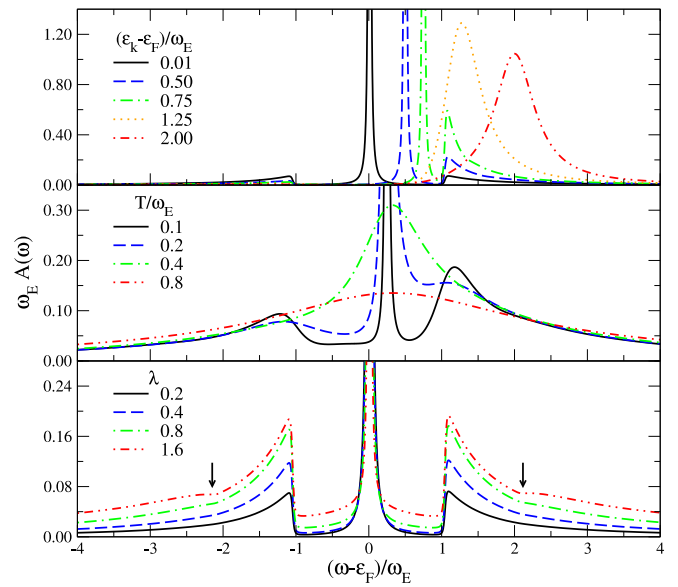


FIG. 3: (color online) Spectral function for the Einstein model using the RC method, where ω_E is the Einstein energy. Top: varying quasiparticle energy for low temperature and weak coupling ($T = 0.01 \omega_E$, $\lambda = 0.2$), middle: varying temperature near the Fermi energy and with medium coupling ($\varepsilon_k - \varepsilon_F = 0.25 \omega_E$, $\lambda = 1.0$), bottom: varying electron-phonon coupling constant at low temperature near the Fermi energy ($\varepsilon_k - \varepsilon_F = T = 0.01 \omega_E$).

IV. RESULTS AND DISCUSSION

In this section, we present illustrative results for several elemental metals and for Einstein and Debye models with a range of electron-phonon couplings over a range of temperatures and energies for both the RC and GW methods.

A. Einstein model

As a first example, we consider the Einstein model self-energy Σ^E , i.e., using the single-pole (zeroth-order Lanczos) approximation for the Eliashberg function,

$$\alpha^2 F(\omega) = \alpha^2(\omega_E) \delta(\omega - \omega_E), \quad (15)$$

where ω_E is the Einstein frequency. For realistic systems, the value of ω_E is taken to be the centroid of the PDOS provided by the ABINIT calculation. As an example, we present results for an Einstein model with $\omega_E = 21.6$ meV (251 K) representative of Cu metal in Fig. 3. Note that phonon satellites in the spectral function are visible only for quasiparticle energies small compared to phonon frequencies $\varepsilon_k < \omega_E$, and very low temperatures (~ 10 K), as seen in the top two panels of Fig. 3. For the Einstein model, the mean coupling constant λ in Eq. (14) is simply $2\alpha^2/\omega_E$, so we can artificially ramp up the coupling by manually setting the value of α^2 . Typically,

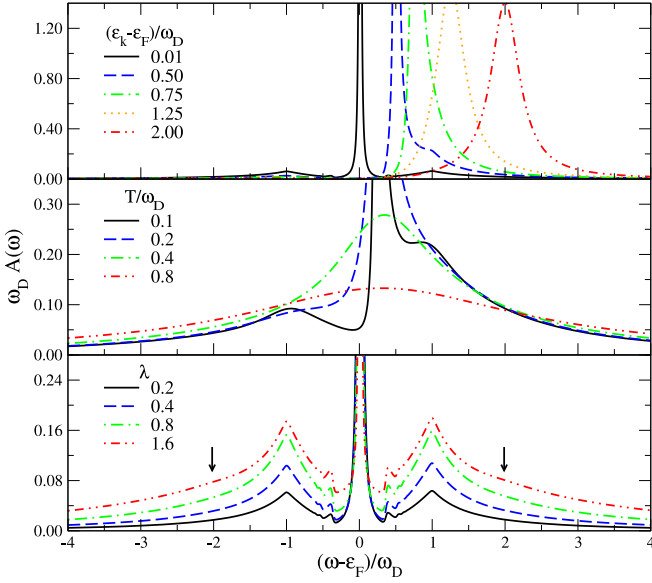


FIG. 4: (color online) Spectral function for the Debye model using the RC method, where ω_D is energy corresponding to the Debye temperature. Top: varying quasiparticle energy for low temperature and weak coupling ($T = 0.01 \omega_D$, $\lambda = 0.2$), middle: varying temperature near the Fermi energy and with medium coupling ($\epsilon_k - \epsilon_F = 0.25 \omega_D$, $\lambda = 1.0$), bottom: varying electron-phonon coupling constant at low temperature near the Fermi energy ($\epsilon_k - \epsilon_F = T = 0.01 \omega_D$).

metals have coupling constants λ that range from roughly 0.1 to 1.7,²⁹ so we will focus on that range. The satellites become larger as λ is increased (third panel), and for $\lambda \approx 1.6$, a weak second phonon satellite becomes apparent at $\omega = \epsilon_F \pm 2\omega_E$. The relative weakness of the 2nd satellite even at $\lambda = 1.6$ suggests Migdal's theorem is valid to high accuracy for typical metals, apart from corrections close to the Fermi energy at very low temperatures.

B. Debye model

For comparison, we show similar results using the Debye model PDOS converted to a many-pole form in Fig. 4, with quantities expressed in terms of the Debye temperature for copper $\Theta_D = 315 \text{ K} = 27.1 \text{ meV} = \omega_D$. Overall, the Debye model shows trends quite similar to the Einstein model. However, the phonon satellites are not as sharply peaked, and the satellites at $2\omega_D$ are barely visible at the same scale for large couplings $\lambda \sim 1.6$. Note that artifacts of the many-pole model can be seen in the spectral functions as small peaks near the Fermi energy (third panel), though these are negligible compared to the phonon satellites.

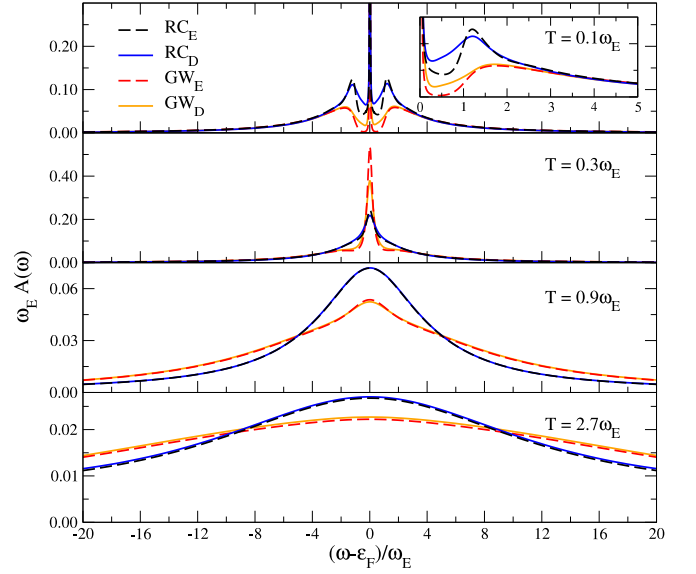


FIG. 5: (color online) Comparison of spectral function from the RC and GW methods using the Einstein and Debye models at strong coupling (i.e., $\lambda = 1.6$) near the Fermi level ($\epsilon_k = \epsilon_F + 0.01 \omega_E$) for various temperatures, where $\omega_D \approx 1.3 \omega_E$. Inset: enlarged view of phonon satellites seen in the top panel. Note the satellite centroid for the GW method is further out, and the kink in the RC satellite at $2\omega_E$.

C. Comparison of RC and GW

We note that the electron spectral function near the Fermi level $k = k_F$ is generally nearly symmetrical due to particle-hole symmetry, and is sensitive to phonon correlations beyond GW at strong electron-phonon coupling, as illustrated by the significant deviation of RC from GW seen in Fig. 5. Thus, it is useful to compare the RC and GW methods in this limit, especially since the differences characterize corrections to the GW approximation due to vertex effects. Fig. 5 shows that the two methods differ significantly at strong couplings and low temperatures compared to the Debye or Einstein temperature (see Table I for distribution of spectral weight). The RC method gives larger satellite weights, with a strong first satellite peak at ω_E and a slight kink at $2\omega_E$ (see Inset to Fig. 5). However, the differences between the two methods diminish as the temperature is increased towards room temperature.

D. Selected metals: Cu, Nb, Pb, Ta, and V

Next, we present results for the spectral function for a few elemental solids (Fig. 6) representative of a range of electron-phonon couplings (See Table II). To obtain the full spectral function for these materials, we use the many-pole representation of Eq. (12) as calculated by FEF9, as shown in Fig. 2 for copper. The results for these metals follow similar trends with the RC and GW

TABLE I: Comparison of weights for the quasiparticle peak, hole satellite, and particle satellite (Z_k, w_h, w_p respectively) using the RC and GW methods, done for the Einstein/Debye models at large coupling ($\lambda = 1.6$) and several elemental metals near the Fermi level at low temperature ($\varepsilon_k = \varepsilon_F + 0.01 \omega_{E,Cu} = 0.216$ meV, $T = 0.1 \omega_{E,Cu} = 25.1$ K).

		Z_k	w_h	w_p	λ
RC	Einstein	0.19	0.39	0.42	1.60
	Debye	0.18	0.39	0.43	1.60
	V	0.29	0.34	0.37	1.17
	Nb	0.31	0.33	0.36	1.08
	Pb	0.35	0.31	0.34	0.95
	Ta	0.37	0.30	0.33	0.91
	Cu	0.85	0.07	0.08	0.16
GW	Einstein	0.38	0.31	0.31	1.60
	Debye	0.37	0.31	0.32	1.60
	V	0.45	0.27	0.28	1.17
	Nb	0.46	0.27	0.27	1.08
	Pb	0.49	0.25	0.26	0.95
	Ta	0.50	0.24	0.26	0.91
	Cu	0.86	0.07	0.07	0.16

methods that we saw with our results for the Einstein and Debye models. Copper, which has a relatively weak coupling ($\lambda \sim 0.1$), displays near agreement between the RC and GW methods. Tantalum and vanadium, on the other hand, have medium to strong couplings, respectively, and show significant differences between the two methods. Most noticeably, for increasing quasipar-

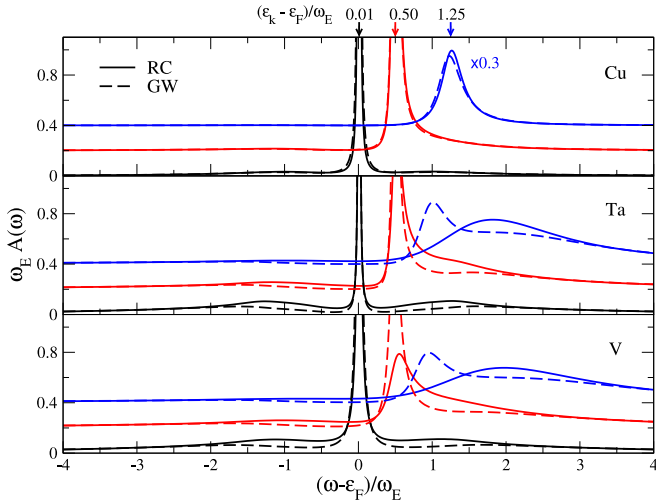


FIG. 6: (color online) Comparing the spectral functions of the RC and GW methods for select metals at low temperature and three quasiparticle energies ε_k for $(\varepsilon_k - \varepsilon_F)/\omega_E = 0.01, 0.5, 1.25$ (bottom, middle, top vertically offset curves respectively in each panel, with arrows indicating corresponding location along the horizontal axis). For Cu, Ta, and V, $\omega_E = 21.6, 15.0, 24.1$ meV respectively and $T = 0.15 \omega_E = 37.65, 17.4, 42.0$ K respectively. The spectral function for Cu with $\varepsilon_k - \varepsilon_F = 1.25 \omega_E$ has been scaled vertically, as indicated.

ticle energies, both the distribution of weight between the quasiparticle and satellites and the location of these peaks disagree significantly, possibly enough to be noticeable experimentally. However, these differences can only be seen at low temperatures (~ 50 K). Even with the strongest coupling, vanadium does not show multiple phonon satellites, indicating Migdal's theorem is valid to high accuracy for phonons in these materials.

E. Comparison with experiment

Evidence for electron-phonon effects in the spectral function have been measured in a number of cases. For instance, the value of the mean coupling constant λ is obtained from the slope of the quasiparticle linewidth $\Gamma \sim 2\pi\lambda k_B T$ versus temperature.¹⁹ Thus, calcula-

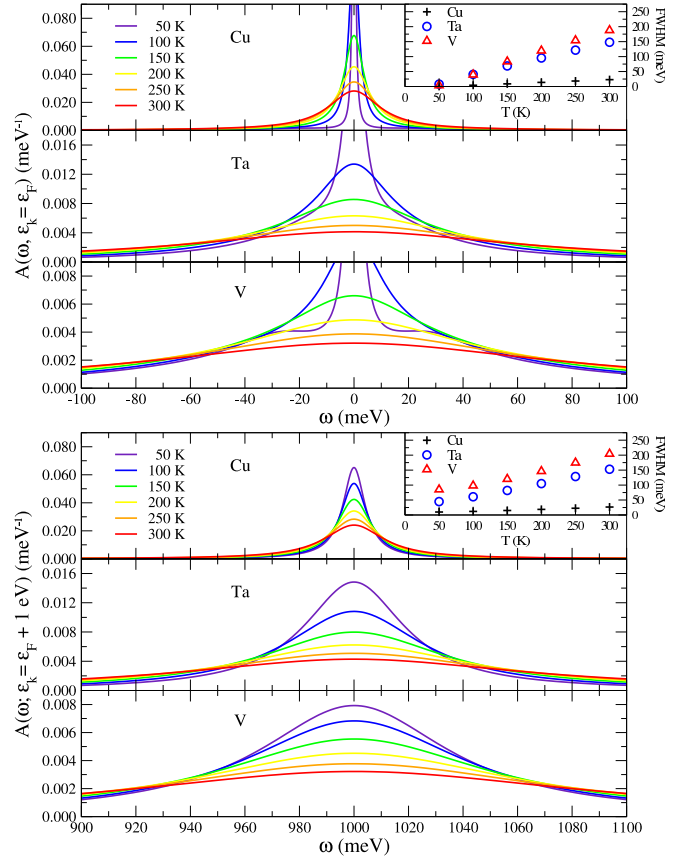


FIG. 7: (color online) Behavior of the quasiparticle peak versus temperature at the Fermi energy $\varepsilon_k = \varepsilon_F$ (top), and at moderate quasiparticle energy $\varepsilon_k = \varepsilon_F + 1.0$ eV (bottom) for Cu, Ta, and V. Insets: Behavior of the quasiparticle widths Γ (FWHM) versus temperature, illustrating how the width of the spectral function grows linearly with T according to $\Gamma \sim 2\pi\lambda k_B T$. This relation can be used to estimate the electron-phonon coupling strength λ (see Table II). Note that the widths at the Fermi energy are significantly reduced at low temperatures compared to those at $\varepsilon_k = \varepsilon_F$, due to the effect of phonon satellites on the distribution of spectral weight.

TABLE II: Calculated electron-phonon coupling constants using two methods—the inverse moment of the many-pole $\alpha^2 F(\omega)$ (Eq. 14) and the temperature dependence of the quasiparticle linewidth taken from the spectral functions at large ε_k —and experimental results for comparison.

	$\lambda^{(\text{MP})}$	λ^Γ	λ^{expt}		
V	1.174	0.899	0.82 ^b	1.09 ^c	0.80 ^d
Nb	1.079	0.897	1.04 ^b	1.06 ^c	1.16 ^d
Pb	0.946	0.955	1.55 ^b	1.48 ^c	1.45 ^d
Ta	0.909	0.809	0.78 ^b	0.87 ^c	
Cu	0.155	0.126	0.10 ^a	0.13 ^c	0.08 ^d

^aRef. 37 ^bRef. 38 ^cRef. 39 ^dRef. 40

tions of quasiparticle linewidths characterize the phonon contributions to the quasiparticle broadening. Our calculated quasiparticle peak FWHM (Fig. 7) are comparable to those measured experimentally.^{41–43} Due to the redistribution of spectral weight from the quasiparticle peak to the phonon satellites at $\varepsilon_k \sim \varepsilon_F$, we use the quasiparticle widths at large ε_k to approximate λ . Taking copper for example, we find a slope of ≈ 0.0680 meV/K, corresponding to $\lambda = 0.126$. The calculated λ for the metals using the quasiparticle linewidths in addition to Eq. (14) are given in Table II, along with several experimental results for comparison. Overall, there is decent agreement with experiment. The heavier metals show more discrepancy, which is likely an effect of the absence of spin-orbit coupling in our simulations.^{44,45}

As another application, the value of electron-phonon coupling is also directly related to the superconducting critical temperature T_c ,^{26,46} i.e.,

$$T_c = \frac{\omega_{\text{ln}}}{1.20} \exp \left[-\frac{1.04(1+\lambda)}{\lambda - \mu^*(1+0.62\lambda)} \right] \quad (16)$$

$$\omega_{\text{ln}} \equiv \exp \left[\frac{2}{\lambda} \int_0^\infty d\omega \frac{\ln(\omega)}{\omega} \alpha^2 F(\omega) \right],$$

where μ^* is the Coulomb pseudopotential, a fitting parameter typically ~ 0.1 - 0.2 .⁴⁷ The T_c calculated for the non-superconducting copper, with $\lambda = 0.155$ and $\mu^* = 0.1$, is extremely low ($\sim 10^{-9}$) as expected. The other metals give T_c on the correct order of magnitude (~ 1 – 10

K), though the calculation is sensitive to the choice of Coulomb pseudopotential.

V. SUMMARY AND CONCLUSIONS

We have implemented a retarded cumulant (RC) expansion approach to calculate phonon contributions to electron spectral function. This approach goes beyond the standard GW approximation to include effects of phonon excitation satellites in the electron spectral function. Our calculations show that the phonon contribution to the quasiparticle peak is linearly dependent on temperature. We verify that Migdal's theorem is generally satisfied for phonons to high accuracy. Thus the effects of vertex corrections leading to deviations between the GW and RC approaches and multiple satellites in the spectral function and are generally negligible except at very low T ($T \lesssim 50$ K) and very strong electron-phonon couplings ($\lambda \gtrsim 1$), and would require roughly meV resolution to discern experimentally. The approach is implemented as part of the AI2PS workflow tool developed by our group.³² This hybrid code takes advantage of the capabilities of both ABINIT and FEFF9 to generate a number of phonon properties, which include x-ray Debye-Waller factors, phonon contributions to the electron self-energy and spectral function, electron-phonon couplings, as well as estimates of the BCS superconductor critical temperatures. With an appropriate self-energy, the method presented here can also be extended to treat insulators and molecular systems.

Acknowledgments

We thank C. Draxl, L. Reining, P. B. Allen, G. Rignanese, X. Gonze, M. Bernardi, and K. Jorissen for useful discussions, and S. R. Williams and J. Vinson for assistance in code development. The ABINIT code is a common project of the Université Catholique de Louvain, Corning Incorporated and other contributors (URL <http://www.abinit.org>). This work was supported in part by DOE grant DE-FG02-97ER45623.

¹ T. Cuk, D. H. Lu, X. J. Zhou, Z.-X. Shen, T. P. Devereaux, and N. Nagaosa, *Physica Status Solidi (b)* **242**, 11 (2005).

² A. Migdal, *Sov. Phys. JETP* **7**, 996 (1958).

³ S. Engelsberg and J. R. Schrieffer, *Phys. Rev.* **131**, 993 (1963).

⁴ M. Bernardi, M. Palummo, and J. C. Grossman, *Nano Lett.* **13**, 3664 (2013).

⁵ D. Y. Qiu, F. H. da Jornada, and S. G. Louie, *Phys. Rev. Lett.* **111**, 216805 (2013).

⁶ M. S. Hybertsen and S. G. Louie, *Phys. Rev. B* **34**, 5390 (1986).

⁷ G. Onida, L. Reining, and A. Rubio, *Rev. Mod. Phys.* **74**, 601 (2002).

⁸ P. B. Allen and B. Mitrović, in *Solid State Physics*, edited by H. Ehrenreich, F. Seitz, and D. Turnbull (Academic Press, 1982), vol. 37 of *Solid State Physics*, pp. 1–92.

⁹ L. Hedin, *J. Phys.: Condens. Matter* **11**, R489 (1999).

¹⁰ P. Steiner, H. Höchst, S. Hüfner, L. Ley, and M. Cardona, *Topics Appl. Phys.* **27**, 349 (1979).

¹¹ F. Offi, W. Werner, M. Sacchi, P. Torelli, M. Cautero, G. Cautero, A. Fondacaro, S. Huotari, G. Monaco, G. Paolicelli, et al., *Phys. Rev. B* **76**, 085422 (2007).

- ¹² O. Gunnarsson, V. Meden, and K. Schönhammer, Phys. Rev. B **50**, 10462 (1994).
- ¹³ R. Kubo, J. Phys. Soc. Jpn. **17**, 1100 (1962).
- ¹⁴ J. J. Kas, J. J. Rehr, and L. Reining (2014), 1402.0022.
- ¹⁵ L. Hedin, Physica Scripta **21**, 477 (1980).
- ¹⁶ F. Aryasetiawan, L. Hedin, and K. Karlsson, Phys. Rev. Lett. **77**, 2268 (1996).
- ¹⁷ M. Guzzo, G. Lani, F. Sottile, P. Romaniello, M. Gatti, J. J. Kas, J. J. Rehr, M. G. Silly, F. Sirotti, and L. Reining, Phys. Rev. Lett. **107**, 166401 (2011).
- ¹⁸ M. Casula, A. Rubtsov, and S. Biermann, Phys. Rev. B **85**, 035115 (2012).
- ¹⁹ G. Grimvall, *The electron-phonon interaction in metals* (North-Holland Amsterdam, 1981).
- ²⁰ A. Eiguren and C. Ambrosch-Draxl, Phys. Rev. Lett. **101**, 036402 (2008).
- ²¹ R. M. Nicklow, G. Gilat, H. G. Smith, L. J. Raubenheimer, and M. K. Wilkinson, Phys. Rev. **164**, 922 (1967).
- ²² L. Hedin and S. Lundqvist, Solid State Physics **23**, 1 (1970).
- ²³ B. Lundqvist, Phys. kondens. Materie. **6**, 193 (1967).
- ²⁴ B. Lundqvist, Phys. kondens. Materie. **6**, 206 (1967).
- ²⁵ J. J. Kas, A. P. Sorini, M. P. Prange, L. W. Cambell, J. A. Soininen, and J. J. Rehr, Phys. Rev. B **76**, 195116 (2007).
- ²⁶ W. L. McMillan, Phys. Rev. **167**, 331 (1968).
- ²⁷ G. Grimvall, Phys. kondens. Materie. **11**, 279 (1970).
- ²⁸ P. B. Allen, Phys. Rev. B **6**, 2577 (1972).
- ²⁹ S. Y. Savrasov and D. Y. Savrasov, Phys. Rev. B **54**, 16487 (1996).
- ³⁰ F. D. Vila, J. J. Rehr, H. H. Rossner, and H. J. Krappe, Phys. Rev. B **76**, 014301 (2007).
- ³¹ P. B. Allen, in *Handbook of Superconductivity*, edited by C. P. Poole (Academic Press, 1999), chap. 9, pp. 478–483.
- ³² More information: <http://www.feffproject.org/>.
- ³³ X. Gonze, J. M. Beuken, R. Caracas, F. Detraux, M. Fuchs, G. Rignanese, L. Sindic, M. Verstraete, G. Zerah, F. Jollet, et al., Comput. Mat. Sci. **25**, 478 (2002).
- ³⁴ X. Gonze, Z. Kristallogr. **220**, 558 (2005).
- ³⁵ J. J. Rehr, J. J. Kas, F. D. Vila, M. P. Prange, and K. Jorissen, Phys. Chem. Chem. Phys. **12**, 5503 (2010).
- ³⁶ M. Methfessel and A. T. Paxton, Phys. Rev. B **40**, 3616 (1989).
- ³⁷ P. Chaikin, G. Arnold, and P. Hansma, J. Low Temp. Phys. **26**, 229 (1977).
- ³⁸ E. L. Wolf, *Principles of electron tunneling spectroscopy* (Oxford Univ. Press, 1985).
- ³⁹ P. B. Allen, Phys. Rev. B **36**, 2920 (1987).
- ⁴⁰ S. D. Brorson, A. Kazeroonian, J. S. Moodera, D. W. Face, T. K. Cheng, E. P. Ippen, M. S. Dresselhaus, and G. Dresselhaus, Phys. Rev. Lett. **64**, 2172 (1990).
- ⁴¹ B. A. McDougall, T. Balasubramanian, and E. Jensen, Phys. Rev. B **51**, 13891 (1995).
- ⁴² A. Eiguren, B. Hellsing, F. Reinert, G. Nicolay, E. V. Chulkov, V. M. Silkin, S. Hüfner, and P. M. Echenique, Phys. Rev. Lett. **88**, 066805 (2002).
- ⁴³ F. Reinert, B. Eltner, G. Nicolay, D. Ehm, S. Schmidt, and S. Hüfner, Phys. Rev. Lett. **91**, 186406 (2003).
- ⁴⁴ M. J. Verstraete, M. Torrent, F. Jollet, G. Zerah, and X. Gonze, Phys. Rev. B **78**, 045119 (2008).
- ⁴⁵ R. Heid, K.-P. Bohnen, I. Y. Sklyadneva, and E. V. Chulkov, Phys. Rev. B **81**, 174527 (2010).
- ⁴⁶ R. Dynes, Solid State Communications **10**, 615 (1972).
- ⁴⁷ P. Morel and P. Anderson, Phys. Rev. **125**, 1263 (1962).